Numerical observation of nonaxisymmetric vesicles in fluid membranes

Yan Jie,[1] Liu Quanhui,[1] Liu Jixing,[1] and Ou-Yang Zhong-Can[1,2]
[1]*Institute of Theoretical Physics, Chinese Academy of Sciences, P.O. Box 2735, Beijing 100080, China*
[2]*Center for Advanced Study, Tsinghua University, Beijing 100084, China*
(Received 19 February 1998; revised manuscript received 8 May 1998)

By means of Surface Evolver, a software package of brute-force energy minimization over a triangulated surface developed by the geometry center of the University of Minnesota [Exp. Math **1**, 141 (1992)], we have numerically searched the nonaxisymmetric shapes under the Helfrich spontaneous curvature (SC) energy model. We show that there are abundant mechanically stable nonaxisymmetric vesicles in the SC model, including both regular shapes with intrinsic geometric symmetry and complex irregular ones. We report in this paper a catalog of interesting shapes including a *corniculate* shape with six corns, a quadriconcave shape, a shape resembling *sickle cells*, a shape resembling *acanthocytes*, and two *tubelike* shapes. Most of these shapes can be related to experimental observations in red blood cells and other experiments in fluid membrane. [S1063-651X(98)06510-6]

PACS number(s): 82.70.−y, 68.15.+e, 02.40.−k

I. INTRODUCTION

Vesicles are bags of lipid bilayer membranes which form spontaneously in an aqueous environment under appropriate conditions. In order to study theoretically the morphology of vesicles, a lipid bilayer with liquid crystalline structures and characteristics has long been considered as a model. A description of a fluid membrane by a curvature energy model was given by Canham [1], in which the local energy density of the form $(2H)^2$ was introduced, where H is the mean curvature of the surface. According to the current viewpoint, this energy model is a faithful description of a vesicle which consists of a symmetric bilayer. However, real lipid bilayers are not symmetric and hence there is no genuine physical realization of this model. Helfrich [2] proposed from curvature elastic theory in liquid crystal the well-known spontaneous curvature (SC) energy model, in which the energy functional is

$$F=\frac{1}{2}\kappa_c\int (C_1+C_2-C_0)^2 dA+\Delta P\int dV+\lambda\int dA, \tag{1}$$

where dA and dV are the surface area and the volume elements for the vesicle, respectively, κ_c is an elastic modulus, C_1 and C_2 are the two principal curvatures of the surface, and C_0 is the spontaneous curvature to describe the possible asymmetry of the bilayer membrane. Nonzero values of C_0 result from the fact that a lipid bilayer may have a tendency to curve one way or the other, due, for example, either to intrinsic chemical asymmetry between the two leaves and/or to a chemical asymmetry between the interior and exterior aqueous environments. The Lagrange multipliers ΔP and λ take account of the constraints of constant volume and area, which can be physically understood as the osmotic pressure between the ambient and the internal environments, and the surface tensile coefficient, respectively. Based on the model, many works on the morphology of vesicles have been done in the axisymmetric case. In their pioneering work on the model, Deuling and Helfrich [3,4] numerically found a catalog of possible axisymmetric vesicle shapes. In their papers they used the nomenclature developed in the red blood cells (RBCs) literature to describe the shapes they found: The prolate and oblate ellipsoid, stomatocytes, and discocytes, some of which strikingly resemble the shapes of human RBCs.

Further, by performing the variation of the energy functional the general equilibrium shape equation was derived [5],

$$\Delta P+2\lambda H-2k_c[2H(H^2-K)+C_0K+(C_0^2/2)H+\nabla^2 H]=0, \tag{2}$$

where $\nabla^2=[(1/\sqrt{g})\,\partial_i(g^{ij}\sqrt{g}\partial_j)]$ is the Laplace-Beltrami operator, g is the determinant of the metric g_{ij}, and $g^{ij}=(g_{ij})^{-1}$, $K=C_1C_2$ is the Gaussian curvature, and $H=(1/2)(C_1+C_2)$ is the mean curvature (here we use a different sign convention for H from the original derivation of the general shape equation in [5]).

By using the scale invariance of the curvature energy functional (1), the number of parameters can be reduced. The area A is often used to define a length scale $R_0=\sqrt{A/4\pi}$, and R_0 is used to define two independent dimensionless variables, the reduced volume $v=V/(4/3)\pi R_0^3$, and the reduced spontaneous curvature $c_0=C_0R_0$. Any solution of Eq. (2) depends only on these two dimensionless quantities. The values of (v,c_0) in general correspond to a set of shapes, denoted by $S_{(v,c_0)}$. For a given value of c_0, it can be qualitatively understood that the number of shapes in $S_{(v,c_0)}$ should increase as v decreases. At the right end, $v=1$, there is only one shape in $S_{(1,c_0)}$, namely, the sphere.

Locating different branches of shapes of minimal energy in the parameter space spanned by (v,c_0), the division of the parameter space represents the so-called phase diagram for the vesicle shapes. In the SC model, Seifert *et al.* [6] calculated the two-dimensional phase diagram for axisymmetric shapes within a limited parameter space.

Solving the shape equation under the axisymmetric case in which the corresponding shape equation can be transformed from Eq. (2) into an ordinary differential equation

[7], several analytical solutions have been found. Among these solutions are the solution of biconcave shape, the torus solution, and the beyond-Delaunay surfaces [8], in which the first two solutions have been supported experimentally [9]. All these studies concentrate on axisymmetric vesicle shapes. No nonaxisymmetric vesicle shape of spherical topology has been reported in the SC model.

On the other hand, in other curvature energy models, some progress has been achieved in finding nonaxisymmetric vesicle shapes of spherical topology by means of brute-force energy minimization over a triangulated surface. In the area difference elastic (ADE) model, nonaxisymmetric ellipsoid shapes have been reported [10], and very recently, Wintz *et al.* [11] reported a catalog of starfish shapes based on a modified ADE model including the contribution of the compressibility of the total area and volume. Characteristic of the starfish shapes is their flatness and their multifold symmetry. As far as we know, no other nonaxisymmetric vesicle shape has been reported in the literature by any of the known models.

However, on the experimental side, various nonaxisymmetric RBC shapes of spherical topology have long been observed. They may take very complex configurations, and many of them even have no intrinsic geometric symmetry. There are a lot of clear figures obtained by scanning electron microscope of RBCs in the book *Living Blood Cells and Their Ultra-structure* [12] including very complex vesicle shapes such as the *echinocyte type* cells (Fig. 98 in [12]) which have a characteristic shape with crenations or spicules (almost) evenly distributed on the surface, the *acanthocyte type* cells (Figs. 157 and 159 in [12]) which bear a superficial resemblance to *echinocytes* but with many fewer spicules irregularly arranged and bent back at their tips, the *knizocytes* (Figs. 106 and 107 in [12]) which are triconcave and quadriconcave shapes, the *sickle type* cells (Fig. 198 in [12]) which show a sicklelike shape, and so on. In addition, many other complex shapes were found in the experimental study of transformation pathways of liposomes [13], in which the shape transformation is induced by the osmotic pressure. A circular biconcave form was used as the initial shape in this study. Many thin stable flexible tube forms were also found. Before the full development of these tubes certain transient forms appear which can be described as filaments with small heads. These tubes are curved, so they are also nonaxisymmetric.

These complex shapes have not yet been understood theoretically in the context of bending energy models. Some researchers [14] believe that such exotic shapes may involve other energy contributions such as higher-order-curvature terms and van der Waals attraction of the membrane. However, the conjecture is not so obvious as it seems. We would like to explore if it is possible to describe these complex shapes by a simple curvature model, such as the SC model. The purpose of this paper is to search numerically for nonaxisymmetric shapes of spherical topology within the framework of the SC model.

Inspired by its success in finding the nonaxisymmetric ellipsoidal and starfish shaped vesicles [10,11], we have employed the algorithm of brute-force energy minimization over a triangulated surface in the present study. The method directly minimizes the total energy. The resulting shape has a local energy minimum which depends in principle on the initial shape chosen.

We will also locate each shape found by us in the phase diagram in order to know to which region of the parameter space these shapes belong. Further, in order to describe the vesicle shapes, we will use the same nomenclature as in [12] for the shapes that resemble the figures in [12].

The plan of the paper follows: Section II describes the algorithm and the procedure; Sec. III gives the main results; and Sec. IV has the discussion and conclusion.

II. MODEL, SOFTWARE, AND THE PROCEDURE

In order to find the locally stable nonaxisymmetric configurations of vesicles, we evaluate the bending energy numerically with the constraint of the constant volume and/or constant area within the SC model. Under the constraint of constant volume V, the parameter λ is understood as the tensile coefficient while under the constraint of constant area A, the parameter ΔP is understood as the osmotic pressure.

The software we used to search for the surfaces is the ''Surface Evolver'' package of computer programs [15] which is based on the discretization of the curvature energy, the area, and the volume on a triangulated surface. The energy in the Evolver can be a combination of surface tension, gravitational energy, squared mean curvature, etc. The constraints can be on vertex positions, or on integrated quantities such as body volume, surface area, etc. The constraints are incorporated in the bending energy. The resulting total energy is minimized by a gradient descent procedure, and the resulting shape is a local energy minimum. These characteristics of the Evolver make it a useful tool for studying nonaxisymmetric shapes in the SC model. In the Evolver the osmotic pressure is denoted by an internal pressure P and it can deal with the following energy functional conveniently:

$$F = m_1 \int (H - H_0)^2 dA + \lambda \int dA - P \int dV, \qquad (3)$$

where m_1 is called the ''weight'' of the bending energy. Under the definition of $H = (1/2)(C_1 + C_2)$, the model is identical to the SC model under the transformations $m_1 = 2\kappa_c$, $P = -\Delta P$, and $H_0 = C_0/2$. No particular units of measurement are used in the Evolver. However, in order to relate the program values to a real situation, all the values ought to be within one consistent unit system.

The software has been employed to deal with many geometric problems such as constant mean curvature surfaces, equilibrium foam structures, etc. for several years [16–18]. It has also been utilized to deal with a wide range of physical problems involving surfaces as shaped by surface tension and bending and other energies for a long time. To study Kelvin's conjecture on minimal surfaces the authors of [19] used the Surface Evolver to produce the minimal structure of flat-sided polyhedral cells. The Surface Evolver was also used to study elasticity of dry foams [20,21] and compressed emulsions [22,23]. Just as an exercise, we tested it for the equilibrium condition of a perfect sphere with a given target volume evolved from a cube in the SC model. The equilibrium condition for the energy functional (3) is

$$-Pr^3+2\lambda r^2+2m_1H_0r(-1+H_0r)=0, \tag{4}$$

where r is the radius of the sphere. This is identical to the results in [5]. With the parameters $m_1=1$, $H_0=1$, $\lambda=2$, and the target volume $V=4.189$, we obtained a stable unit sphere from the Surface Evolver with the area $A=12.5774$, and the Lagrange multiplier $P=4.0023$, which do satisfy the equilibrium condition.

Though the surfaces found by such an algorithm correspond to the energy minima, the Surface Evolver has a provision to test the stability by subjecting the resulting shapes to a perturbation of finite amplitude. Each vertex of the triangulated surface is moved by $\mathbf{A}\sin(\boldsymbol{\nu}\cdot\boldsymbol{\omega}+\psi)$, where $\mathbf{A}$ is the amplitude vector, $\boldsymbol{\nu}$ is the position vector of the vertexes, $\boldsymbol{\omega}$ is the wave vector, and ψ is the phase. The parameters $\mathbf{A}$, $\boldsymbol{\omega}$, and ψ can be set by hand or generated randomly. In the random cases, a random amplitude $\mathbf{A}$ and a random wavelength L are chosen from a sphere whose radius is the size of the object. We used this feature of the Surface Evolver to test all the shapes reported in the paper.

One should keep in mind two important points of this algorithm. (1) A data file describing the initial shape must be provided in order to initiate the Surface Evolver. It is quite difficult to write the data file for a complex shape. Polyhedra are often used as initial shapes from which a target shape satisfying the constraints, such as target volume, target area, etc., can be obtained by refining and evolving commands of the software. (2) The final shape satisfying the constraints strongly depends on the choice of the initial shape. One may expect that all the possible shapes in a parameter range $v_1 \leqslant v \leqslant v_2$ and $c_{0_1} \leqslant c_0 \leqslant c_{0_2}$ can be found by scanning the region step by step from an initial shape. However, this does not happen because (a) for any pair of values of (v,c_0), there is in general a set of coexisting stable shapes (the coexisting shapes means the shapes with the same parameter values) and (b) the shape found by the algorithm depends strongly on the initial shape. Thus the shapes generated by the scanning method form just a subset of all the possible shapes. Since normally one can write only a simple data file for the starting shape, it is difficult to obtain complex shapes by the scanning procedure. Consider the following example: from a starting shape (which can be stable or unstable), with C_0 and A constant, by gradually changing the value of the target volume V, one can get a sequence of stable shapes (the sequence does not include the initial shape). However, since the $(i+1)$th shape is determined by the ith shape, the whole sequence of generated shapes is determined by the starting shape. A very important point is that the sequence of the generated shapes is insensitive to the initial shape, in that the same sequence is obtained even if the initial shape is slightly distorted. The above scanning process of the example is equivalent to scanning step by step along the reduced volume while the reduced spontaneous curvature is kept constant. However, since for any given pair of values of (v,c_0), there exists a set of coexisting shapes $S_{(v,c_0)}$, it is obvious that the shapes included in the sequence form just a subset of all the shapes existing in the scanning region. Many (complex) shapes will not show up since in general one can only provide a simple datafile for the initial shape. To get complex shapes from the simple initial shapes, the sequence's insensitiveness to the initial shape must be broken.

We suggest the following alternative procedure: if some geometric quantities, such as the volume, the area, the reduced volume, etc., of the target shape are chosen to be far from the initial shape, one can imagine that the initial shape will evolve continuously through a long and complex pathway before it finally reaches a stable configuration satisfying all the geometric constraints. Any configuration in the pathway is unstable. One should expect the final shape (as well as the pathway) to be sensitive to the initial shape due to its long and complex pathway. Two shapes only slightly different from each other may lead to two very different final shapes with the same target constraints since the small difference will be enlarged in the course of evolution.

Hence, from an initial shape with parameters (v_i,c_0), there exist different ways to obtain a final shape with target parameters (v_f,c_0). (a) The shape transition procedure: scanning from v_i to v_f gradually. The shape at each scanning step is stable and the final shape is insensitive to the initial shape. (b) The ''jump'' procedure: an initial shape evolves directly into a final shape with the target parameters, which is sensitive to the initial shape. The two procedures may produce different final shapes coexisting at the same parameters from the same initial shape. Obviously, the jump procedure provides us with the ability to obtain complex shapes from simple initial shapes. Using shapes found by the jump procedure as the initial shapes, more interesting shapes can be generated using the shape transition procedure.

However, there is a technical difficulty with the jump procedure described above: changing the reduced volume abruptly imposes constraints on both the area A as well as the volume V, which often lead to a singular behavior of the software. The Surface Evolver may not converge within a finite number of iterations and singularities might occur. To avoid this problem, we free the constraints on area and abruptly change the volume V to a value far from the initial one. The Surface Evolver thus gains much more freedom to deform the shape in the process of evolving and works with many fewer singularities.

We calculated the reduced spontaneous curvature and the reduced volume for the shapes and located them in the parameter space spanned by (v,c_0) in order to know in which region of the parameter space these shapes exist. Following is an outline of the procedure (supposing we start from a sphere of volume 1).

(i) Given certain values of C_0 and λ, let the Surface Evolver evolve the sphere to a target shape with volume V, where V is far from 1. Here λ is the tensile coefficient, and C_0 is the spontaneous curvature. It is hoped that such a sudden and big change in the volume will trigger a ''random walk'' in the configuration space of the surface shapes before it finally settles in a nontrivial locally stable configuration with volume V. This procedure can be applied to any shape to generate more stable shapes.

(ii) We choose the complex shapes obtained in the above process and study their shape transition sequences, which can generate more stable and interesting shapes.

III. MAIN RESULTS

By the procedure described in the preceding section, many striking vesicle shapes were found. Some of the shapes

resemble the RBC shapes observed experimentally while some resemble the experimental results of liposomes. To describe these exotic shapes, we adopt the nomenclature used in the red blood cells literature for those resembling the observations in RBCs. We report six types of shapes in this paper, the corniculate shape, the knizocyte type shape, the sickle type shape, the acanthocyte type shape, and two tube-like shapes shown in Fig. 1(a), Fig. 2, Fig. 3, Fig. 4, and Fig. 5(a), Fig. 5(b), respectively. Two thousand to 3000 grid points were used with an accuracy of at least 1% in the total energy.

Though the shapes searched by the algorithm are locally stable, the stability was further tested by subjecting them to perturbations of finite amplitude. All the six shapes are stable under the perturbations. Each of the shapes is mapped into the two-dimensional phase diagram following Seifert *et al.* [6] in reduced volume and the scaled spontaneous curvature.

Corniculate shape

Figure 1(a) shows a corniculate surface with six corns, whose location in the phase diagram is ($v=0.95$, $c_0=1.35$). This shape apparently has rotational symmetry which is identical to the octahedron and thus isomorphic to S_4, where S_X denotes the group of permutations of the set X [24]. Though we did not find a similar shape in [12], this shape may indicate the way of formation of echinocyte III vesicle shapes (Fig. 98– Fig. 100 in [12]) which have 10–50 corns evenly distributed on a nearly spherical surface. To show the fact that there are coexisting shapes in the parameter space spanned by (v,c_0), keeping (v,c_0) constant, we subjected the shape shown by Fig. 1(a) to long wavelength perturbation with large amplitude. It is heavily deformed into a distorted one, shown by Fig. 1(b). Running the Surface Evolver on the deformed shape, we finally got a new stable shape shown by Fig. 1(c), an axisymmetric ellipsoidlike shape which has the same parameters as those of Fig. 1(a). Since Fig. 1(a) and Fig. 1(c) are at the same location in the parameter space, we use the mark ''$*1$'' in Fig. 6 to denote both the shapes. It is obvious that the two coexisting stable shapes will lead to two different shape transition sequences under the same transition procedure.

Knizocyte type shape

Knizocytes (Figs. 106 and 107 in [12]) are triconcave and quadriconcave shapes found in the experiments of RBCs. The shape denoted by Fig. 2 is a quadriconcave shape and bears a resemblance to the experimentally observed shape (Fig. 106 in [12]). Its location in the phase diagram is ($v=0.84$, $c_0=-1.41$), denoted by ''$*2$'' in Fig. 6. The shape has rotational symmetry which is identical to a cube and is also isomorphic to S_4 [24]. This shape may be seen under different circumstances. In fresh blood, it may be observed in certain hemolytic anemias. In addition, if a suspension of cells is examined between slide and coverslip and an erythrocyte permitted to adhere to the slide, gentle deformation of the cell by a current of liquid in the preparation may produce this appearance [25].

Sickle type shape

Figure 3 bears the resemblance of the sickle cells in echinocytic forms (Fig. 198 in [12]). The location in the phase

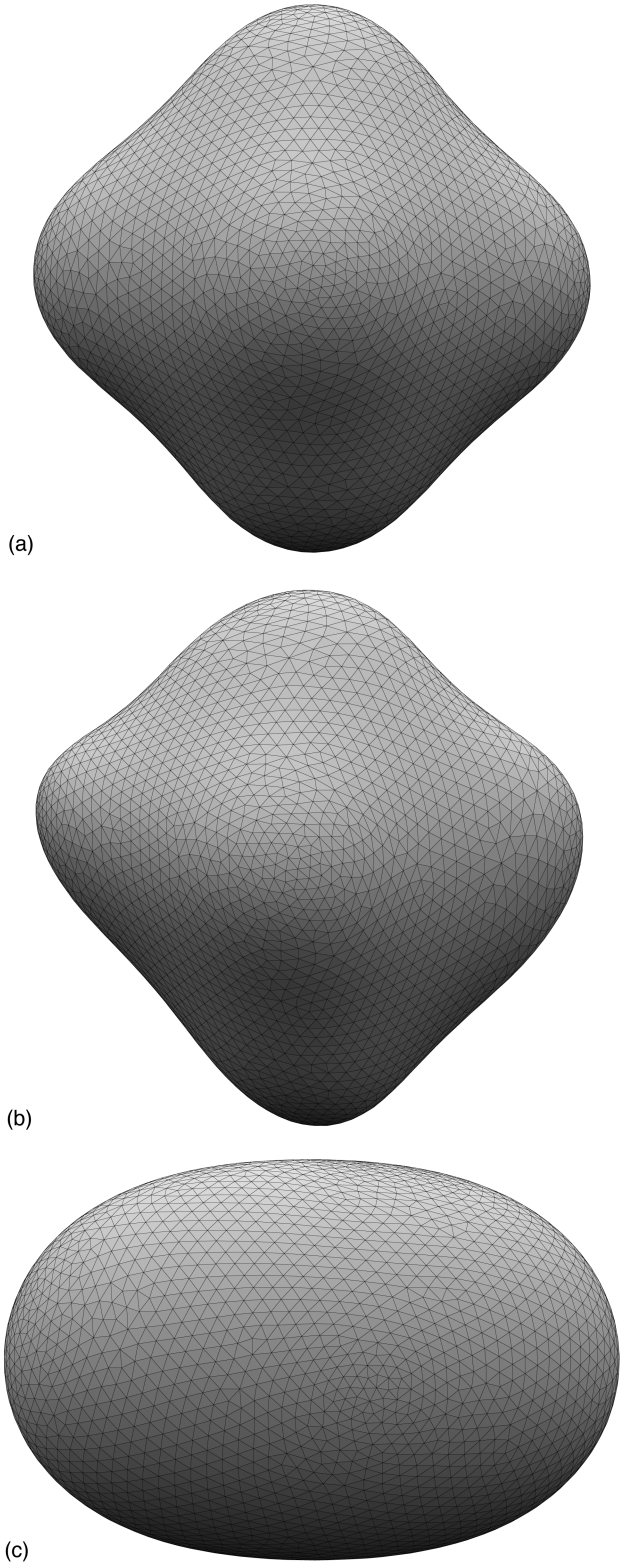

FIG. 1. (a) A corniculate shape at reduced volume $v=0.95$ and reduced spontaneous curvature $c_0=1.35$. (b) A heavily distorted shape after subjecting the corniculate shape to perturbations of large amplitude. (c) An axisymmetric ellipsoid evolved from a distorted shape with the same values of reduced volume and reduced spontaneous curvature as (a).

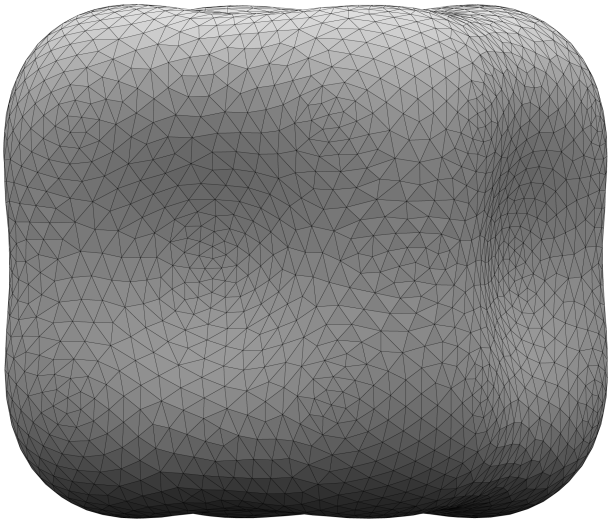

FIG. 2. A quadriconcave shape at reduced volume $v=0.84$ and reduced spontaneous curvature $c_0=-1.41$.

diagram is ($v=0.74$, $c_0=-1.48$) and is denoted by ''∗3'' in Fig. 6. Sickle cell is related to sickle cell disease, a hereditary abnormality. Sickle cells appear when affected blood is exposed to a sufficiently low oxygen tension. The phenomenon can also be seen by sealing a preparation between slide and coverslip and waiting a few hours or leaving the blood for 24 to 48 hours in a vessel without oxygen [26].

Acanthocyte type shape

Figure 4 shows a strikingly complex shape without any intrinsic geometric symmetry. Characteristic of this shape is its irregular shape and several irregularly distributed crenations, which are the same as the so-called acanthocyte type cell shapes (Figs. 157 and 159 in [12]) observed experimentally in RBCs. The location of this shape in Fig. 6 is ($v=0.39$, $c_0=1.35$) denoted by ''∗4.'' It is obtained by a shape transition procedure starting from Fig. 1(a) by gradually increasing the reduced volume v. The designation acanthocyte was given by Singer *et al.* [27] to crenated red cells

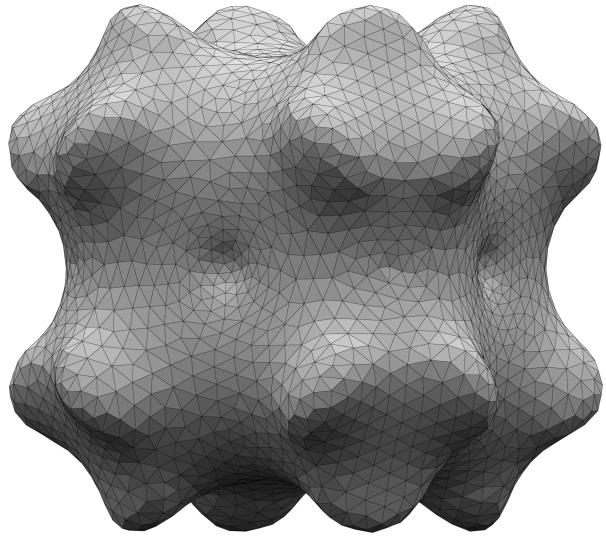

FIG. 3. A sickle type shape at reduced volume $v=0.74$ and reduced spontaneous curvature $c_0=-1.48$.

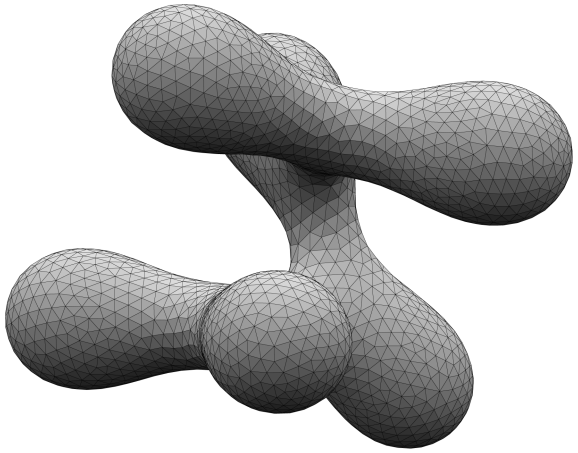

FIG. 4. An acanthocyte type shape obtained by gradually reducing the reduced volume, while the reduced curvature is kept constant, as in Fig. 1(a). The reduced volume is $v=0.38$ and reduced spontaneous curvature $c_0=1.35$.

found in a hereditary illness now characterized by the absence of beta-lipo-protein and serious nervous system alterations. The abnormality appears to develop during the lifespan of the cells within the circulation and to be absent or minimal in the youngest cells [28]. Such complex irregular acanthocyte type shapes are found to be abundant in our study.

Tubelike shapes

Figures 5(a) and 5(b) are two interesting shapes: a curved tubelike tail with a biconcave head and a tubelike shape without a distinct head, respectively. Their parameters are

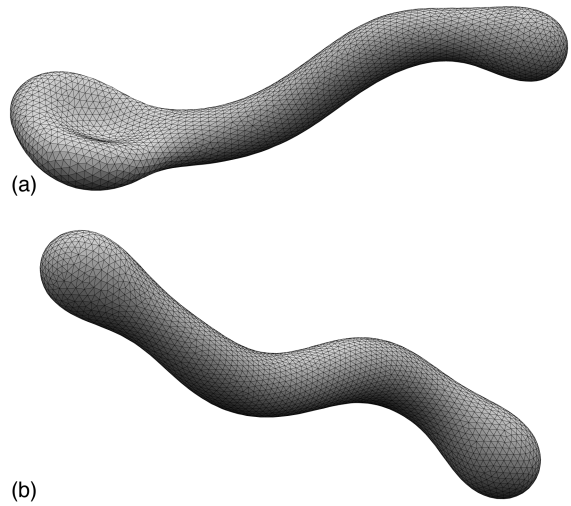

FIG. 5. (a) A tubelike shape with a biconcave head at reduced volume $v=0.38$ and reduced spontaneous curvature $c_0=1.35$. (b) A tubelike shape without a distinct head at reduced volume $v=0.46$ and reduced spontaneous curvature $c_0=1.35$. The two shapes belong to the shape transition sequence starting from Fig. 1(c) and gradually reducing the reduced volume, while the reduced curvature is kept constant. It is not surprising to see that (a) is coexisting with Fig. 4 which belongs to the shape transition sequence starting from Fig. 1(a), since Fig. 1(a) and (a) are coexisting shapes.

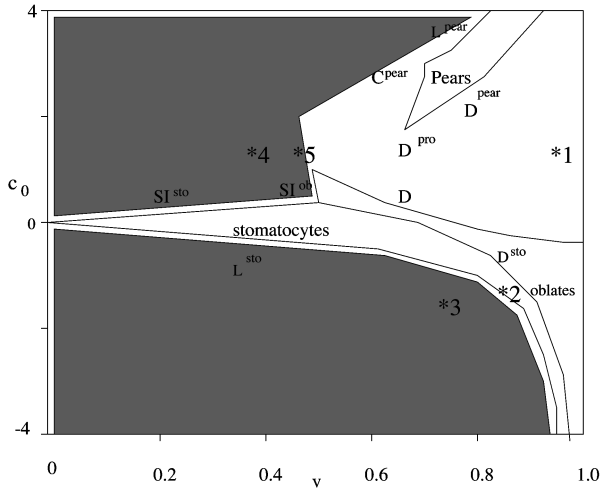

FIG. 6. The schematic copy of the phase diagram in the SC model reproduced by permission of the authors [6]. The phase diagram shows the shape of lowest curvature energy as a function of the reduced volume v and the reduced spontaneous curvature c_0. The regions where the prolate/dumb-bell, pear-shaped, oblate/discocyte, and stomatocytes are stable are separated by transition lines. The shapes included in the initial phase diagram are all axisymmetric, and the shaded regions are those that have not been explored by previous studies. We plot in the phase diagram the locations of the shapes found in the study in order to know to which region these shapes belong. They are denoted by $*n$ where n is an integer. $*1$ corresponds to the two coexisting shapes Fig. 1(a) and Fig. 1(c); $*2$ corresponds to Fig. 2; $*3$ corresponds to Fig. 3; $*4$ corresponds to two existing shapes Fig. 4 and Fig. 5(a). $*5$ corresponds to Fig. 5(b).

($v=0.38$, $c_0=1.35$) and ($v=0.46$, $c_0=1.35$), respectively. Obviously, Fig. 5(a) is coexisting with Fig. 4 and its location is also denoted by ''$*4$'' in the phase diagram. Figure 5(b) is denoted by ''$*5$'' in the phase diagram. The two shapes were obtained by a shape transition procedure starting from Fig. 1(c) and by increasing the reduced volume v gradually. In the study of the transformation pathway of liposomes [13], Fig. 5(b) was experimentally observed as a stable shape. Figure 5(a) was also obtained in the same experiment but only as a transient shape before the final state [Fig. 5(b)] was achieved. However, according to our study, both shapes of Fig. 5(a) as well as Fig. 5(b) are found stable. There are two possible explanations to account for the discrepancy with the experimental observations: (1) there may exist other energy contributions in such a tiny size which prevent Fig. 5(a) from being stable in experiments; (2) by changing the experimental condition, stable configurations like Fig. 5(a) may become stable.

Similar observations were also made in the experiments in RBCs. The book [12] provides many examples of vesicles with tubelike tails and various kinds of head shapes. We find that Fig. 182 of [12], which denotes a kind of poikilocytes in the discocytic form, resembles Fig. 5(a). Poikilocytes are related to the thalassemia disorders or Mediterranean anemias. They take on a variety of bizarre erythrocyte shapes. Though the example is not ''identical'' to Fig. 5(a) from the appearance, it indicates that the latter assumption may be correct, i.e., Fig. 1(a) may be stable under certain conditions.

IV. DISCUSSION AND CONCLUSIONS

The algorithm used in this study has the ability to find complex vesicle shapes starting from simple initial ones under the jump procedure described in the paper. With these complex shapes as the starting shapes, more complex shapes are generated by the shape transition procedure. Many strikingly complex shapes have been found within the framework of the SC model. Some of the shapes searched bear resemblance to experimental observations. Apparently the procedure is also useful in searching new shapes of high genus and can be used in other curvature models. Among the shapes provided in this paper, we have the strong impression of the existence of complex irregular shapes such as the acanthocyte type shapes and curved tubelike shapes, in the SC model, because they are the first reported irregular shapes of spherical topology in a simple curvature energy model. Our study shows that adding new energy contributions, such as higher-order-curvature terms and van der Waals attraction of the membrane, is not necessary to account for such abnormal shapes. In fact, we have also obtained several other irregular shapes which are not included in this paper.

The reason why these shapes may have not been reported by other researchers also employing the same algorithm may be simple: most complex configurations will not show up in the shape transition procedure if the starting shape is simple. In fact, since a pair of values of (v,c_0) corresponds to a set of coexisting shapes, the coexisting shape transition sequences also exist. In fact, Fig. 4 belongs to the shape transition sequence starting from the shape of Fig. 1(a), while Fig. 5(a) and Fig. 5(b) belong to the sequence starting from Fig. 1(c). Since Fig. 1(a) and Fig. 1(c) are two coexisting shapes, the two sequences are also coexisting.

ACKNOWLEDGMENTS

We are indebted to Professor Ken Brakke, Professor Karsten Grosse-Brauckmann, and Professor Rob Kusner for their guidance with the software and for useful suggestions, and to Dr. Seifert for the permission to copy the phase diagram as shown in Fig. 6. We thank Professor Vipin Srivastava for his discussions and a critical reading of the paper, and thank Dr. Zhou Haijun and Dr. Zhao Wei for fruitful discussions. This work is partly supported by the National Natural Science Foundation of China.

[1] P. B. Canham, J. Theor. Biol. **26**, 61 (1970).
[2] W. Helfrich, Z. Naturforsch. C **28**, 693 (1973).
[3] H. J. Deuling and W. Helfrich, Biophys. J. **16**, 861 (1976).
[4] H. J. Deuling and W. Helfrich, J. Phys. (Paris) **37**, 1335 (1976).
[5] Ou-Yang Zhong-Can and W. Helfrich, Phys. Rev. Lett. **59**,

2486 (1987); Phys. Rev. A **39**, 5280 (1989).
[6] U. Seifert, K. Berndl, and R. Lipowsky, Phys. Rev. A **44**, 1182 (1991).
[7] Hu Jian-Guo and Ou-Yang Zhong-Can, Phys. Rev. E **47**, 461 (1993).
[8] H. Naito, M. Okuda, and Ou-Yang Zhong-Can, Phys. Rev. E **48**, 2304 (1993); Ou-Yang Zhong-Can, Phys. Rev. A **41**, 4517 (1990); H. Naito, M. Okuda, and Ou-Yang Zhong-Can, Phys. Rev. Lett. **74**, 4345 (1995).
[9] M. Mutz and D. Bensimon, Phys. Rev. A **43**, 4525 (1991); A. S. Rudolph, B. R. Ratna, and B. Kan, Nature (London) **352**, 52 (1991); Z. Lin, R. M. Hill, H. T. Davis, L. E. Scriven, and Y. Talmon, Langmuir **10**, 1008 (1994).
[10] M. Jaric, U. Seifert, W. Wintz, and M. Wortis, Phys. Rev. E **52**, 6623 (1995).
[11] M. Wintz, H. G. Döbereiner, and U. Seifert, Europhys. Lett. **23**, 404 (1996).
[12] M. Bessis, *Living Blood Cells and their Ultrastructure* (Springer-Verlag, Berlin, 1973).
[13] H. Hotani, J. Mol. Biol. **178**, 113 (1984).
[14] L. Miao, U. Seifert, M. Wortis, and H. G. Döbereiner, Phys. Rev. E **49**, 5389 (1994).
[15] K. Brakke, Exp. Math. **1**, 141 (1992).
[16] Lucas Hsu, Rob Kusner, and John Sullivan, Exp. Math. **1** (3) (1992). This journal is easily available free of charge from http.//www.expmath.org.
[17] K. G. Brauckmann and K. Pothier, Exp. Math. **6** (3) (1997). This journal is easily available free of charge from http://www.expmath.org.
[18] R. Phelan, D. Weaire, and K. Brakke, Exp. Math. **4** (3) (1997). This journal is easily available free of charge from http://www.expmath.org.
[19] D. Weaire and R. Phelan, Philos. Mag. Lett. **69**, 107 (1994).
[20] Douglas A. Reinelt and Andrew M. Kraynik, J. Fluid Mech. **311**, 327 (1996).
[21] Andrew M. Kraynik and Douglas A. Reinelt, J. Colloid Interface Sci. **181**, 511 (1996).
[22] Martin-D. Lacasse, Gary S. Grest, Dov Levine, T. G. Mason, and D. A. Weitz, Phys. Rev. Lett. **76**, 3448 (1996).
[23] Martin-D. Lacasse, Gary S. Grest, and Dov Levine, Phys. Rev. E **54**, 5436 (1996).
[24] M. A. Armstrong, *Groups and Symmetry* (Springer-Verlag, Berlin, 1988).
[25] M. Bessis, *Living Blood Cells and Their Ultrastructure* (Springer-Verlag, Berlin, 1973), pp. 153 and 154.
[26] M. Bessis, *Living Blood Cells and Their Ultrastructure* (Springer-Verlag, Berlin, 1973), p. 240.
[27] K. Singer, B. Fisher, and M. A. Perlstein, Blood **7**, 577 (1952).
[28] C. Reed, P. Ways, and E. Simon, Nouv. Rev. Fr. Hematol. **3**, 59 (1963).